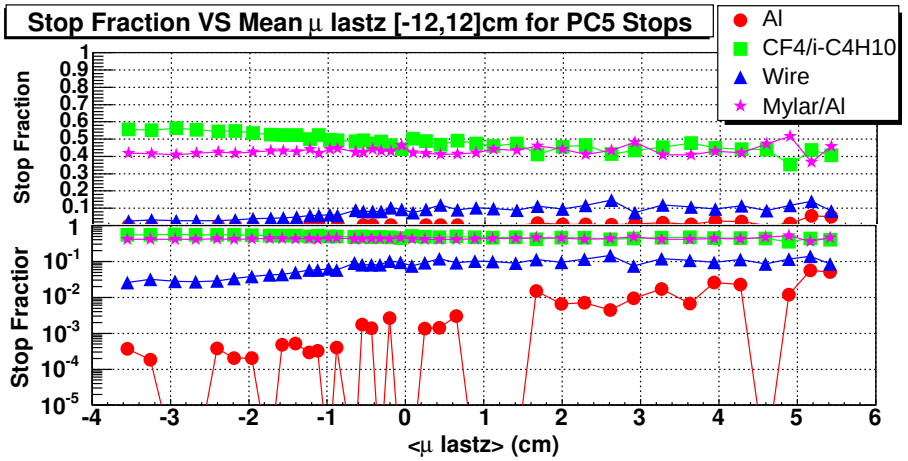

Figure 6.3: Plot of the fraction of muons stopping in Aluminum (Al), Gold plated Tungsten wire, CF4/i-C4H10, and Aluminized Mylar foil for muons with last TDC hit in PC5, versus the mean muon stopping z coordinate between -12.cm and 12.cm from TDC information.

From the PC5 stops data, we can then extract the depolarization in gas by comparing the spectrum for muon last hit in PC6 from this set and from our sets where the muons are stopping at 3/4 in the target. We can write the fit parameter as:

$$\Delta P_\mu^{32-\frac{3}{4}} = P_\mu^{set32} - P_\mu^{stop\frac{3}{4}} \tag{6.6}$$

$$= (f_g^{32} - f_g^{\frac{3}{4}})P_\mu^g + (f_m^{32} - f_m^{\frac{3}{4}})P_\mu^m, or \tag{6.7}$$

$$P_\mu^g = \frac{\Delta P_\mu^{32-\frac{3}{4}} - (f_m^{32} - f_m^{\frac{3}{4}})}{(f_g^{32} - f_g^{\frac{3}{4}})} \tag{6.8}$$

Again using the fractions of muon stops in different materials from Figure 6.2, we get $P_\mu^g = 10.56\Delta P_\mu^{32-\frac{3}{4}} + 1$. This means that if we get a statistical error on our fit of ± 0.0002, then our error on P_μ^g is about 2%. For 5.5% stops in gas, this results in a systematic error of $0.055 \times 0.02 = 0.0011$. It would be nice to find a way to reduce our systematic error, since this method leaves us with a dominant systematic error due to our uncertainty in material depolarization.

Depolarization in Aluminum

A depolarization versus decay time has been observed for muons stopping in our aluminum target. Plots of the polarization estimate from an asymmetry analysis of the 2004 data at the top, and 2004 MC at the bottom are shown in

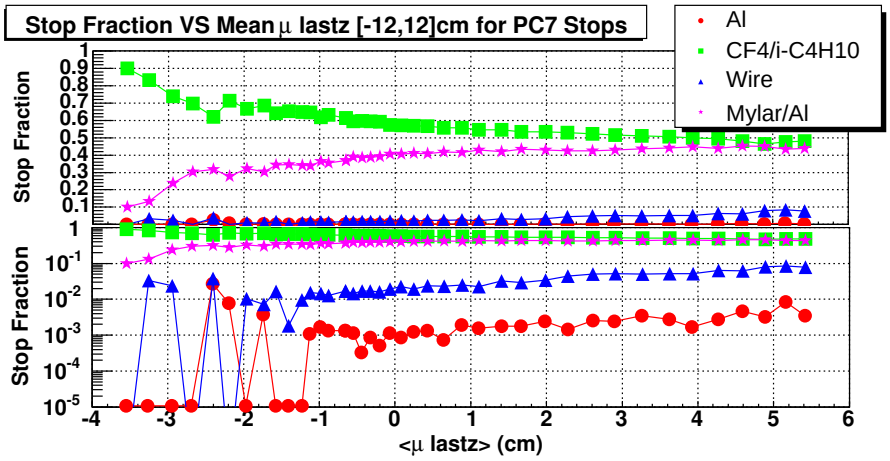

Figure 6.4: Plot of the fraction of muons stopping in Aluminum (Al), Gold plated Tungsten wire, CF4/i-C4H10, and Aluminized Mylar foil for muons with last TDC hit in PC7, versus the mean muon stopping z coordinate between -12.cm and 12.cm from TDC information.

Figure 6.5. The depolarization rate cannot be explained solely by muons that stop in gas rather than aluminum. Models for depolarization in metal are either of an exponential or gaussian form. Calculations have shown that the only practical form is an exponential, since the effects of the other models cannot be very large.

The difference between the two model extrapolations is $2.4 \times 10^{-}3$, and this difference is the *correction* that we need to apply to our MC to data fits, since the MC was generated with a gaussian form, and we want to fit to an exponential form. An estimate of the extrapolation error is obtained by comparing fits with the slope as a fit parameter, and fits with the slope fixed as shown in Figure 6.6. The error due to extrapolation is: $\sqrt{0.00099^2 - 0.00049^2} = 0.00085$.

6.1.2 Fringe Field Depolarization

In this section the sensitivity and systematic error of $P_\mu \xi$ due to uncertainty in beam position and angle is estimated. The uncertainty in beam measurement is estimated in the apparatus section describing the TEC. The uncertainty in the beam position was estimated to be $\pm 2mm$, and the uncertainty in the beam angle was estimated to be $\pm 5mrad$. While this seems like a fairly large uncertainty it is in line with discrepancies between the muon beam position in the detector in MC and data as shown in Figure 6.7.

To estimate the sensitivity to fringe field depolarization, the beam input into MC was scanned over the range $\pm 2cm$ and $\pm 20mrad$ in both x and y. The result of this scan shows that the polarization versus beam shift can be approximated

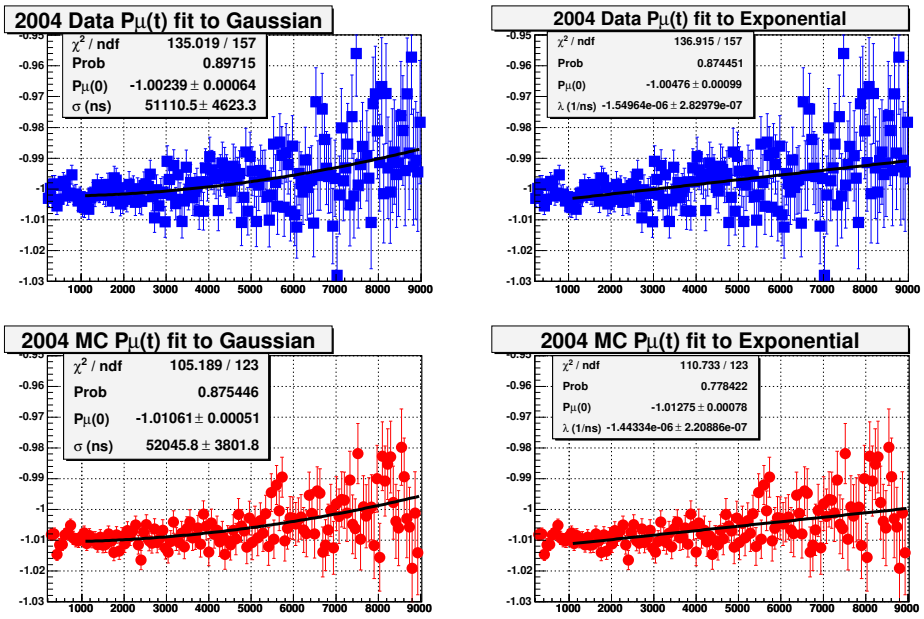

Figure 6.5: Plot of the polarization estimate from an asymmetry analysis of the 2004 data at the top, and 2004 MC at the bottom. The distributions are fit to a gaussian on the left and to an exponential on the right.

by a quadratic polynomial. The scan results are shown in Figure 6.8.

The quadratic that was fit to is given in Equation 6.9, where the x, y, dx and dy represent the shifts in the positions and angles.

$$P_\mu(x, y, dx, dy) = P_{max} - A((dx - x_0)^2 + (dy - y_0)^2) \tag{6.9}$$

The fit constants P_{max} and A were roughly independent of the shift in x and y, while the fit constants x_0 and y_0 were found to be functions of x and y. The polynomial fits are shown in Figure 6.9.

Fits to x_0 versus x and y, and y_0 versus x and y can be done to find the constants in the linear equations:

$$x_0 = x_{00} + x_{0x}x \tag{6.10}$$
$$x_0 = x_{00} + x_{0y}y \tag{6.11}$$
$$y_0 = y_{00} + y_{0x}x \tag{6.12}$$
$$y_0 = y_{00} + y_{0y}y \tag{6.13}$$

The fits to these linear equations are shown in Figure 6.10.

The overall four dimensional polynomial can be written out:

$$P_\mu(x, y, dx, dy) = P_{max} - A((dx - x_{00} - x_{0x}x - x_{0y}y)^2 + (dy - y_{00} = y_{0x}x - y_{0y}y0)^2) \tag{6.14}$$

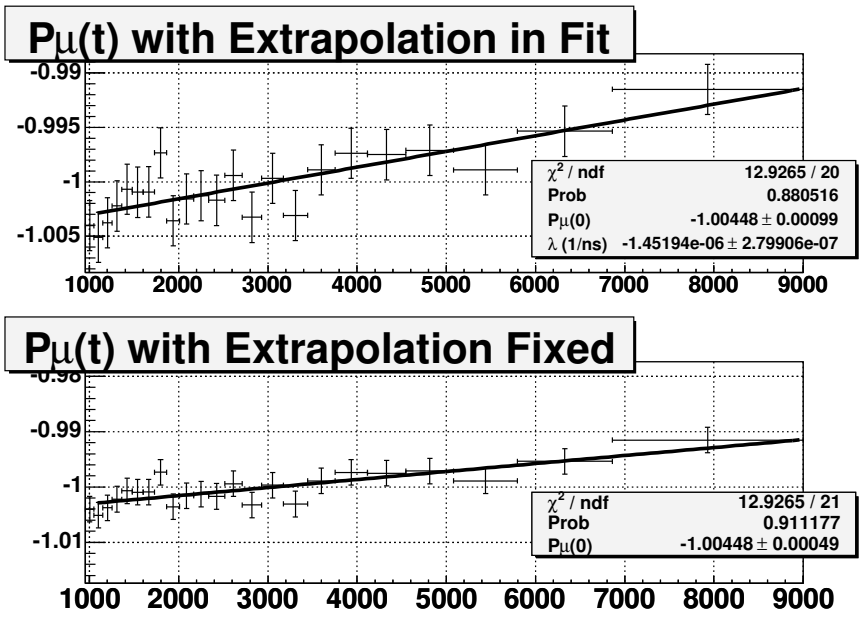

Figure 6.6: Plot of the polarization estimate from an asymmetry analysis of the 2004 data fit to an exponential with the slope as a fit parameter in the top figure, and with the slope fixed in the bottom figure.

The constants in this polynomial for the standard beam tune are summarized in the table below:

The four dimensional polynomial can be used to plot the sensitivity of the polarization to the estimated shifts in the beam. The result is that for an uncertainty in the beam position of $\pm 2mm$, and uncertainty in the beam angle of $\pm 5mrad$, the systematic error in $P_\mu \xi$ ± 0.0015. The plot of the four dimensional polynomial used for this error estimate is shown in Figure 6.12.

6.1.3 Depolarization in the Muon Production Target

6.1.4 Cloud Muon Contamination

6.1.5 Proton Beam Stability

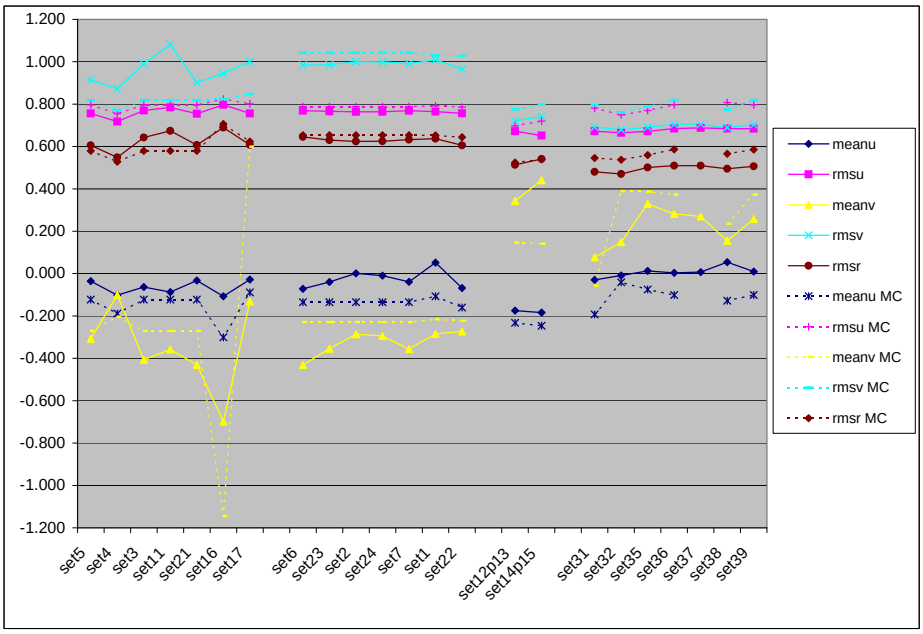

Figure 6.7: This plot shows the match between the mean beam positions and RMS at the stopping target. The match between the two is shown for each of the data sets being considered.

Parameter	Value	Units
P_{max}	0.9958	
A	-9.7960	rad^-2
x_{00}	0.0075	rad
x_{0x}	-0.0129	rad/cm
x_{0y}	-0.0032	rad/cm
y_{00}	0.0058	rad
y_{0x}	0.0024	rad/cm
y_{0y}	-0.0137	rad/cm

Table 6.2: Beam polarization polynomial parameters from fit to MC scan.

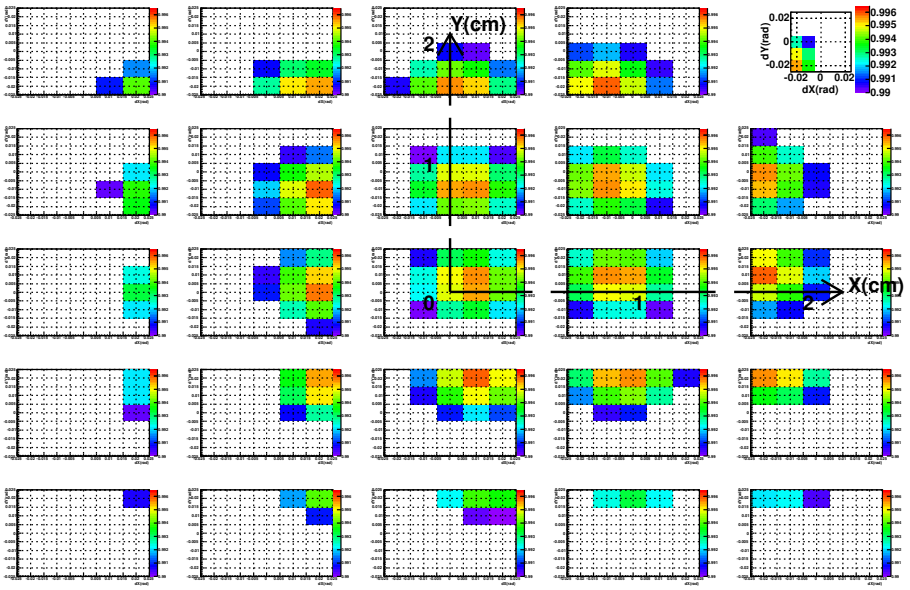

Figure 6.8: Fringe Field Sensitivity MC Scan showing the mean spin along the z axis for muons that stop in the target, where red is the highest polarization of 0.965, and blue is the lowest polarization of 0.99. An unshaded or white square is lower polarization than 0.99. Each of the 25 plots shown here is a polarization for each shift in dY versus dX from +20 mrad to -20mrad. The middle plot is for an unshifted beam, plots on the first row are for the beam shifted up by 2cm at the TEC, the second row shifted up by 1cm, and so on filling the matrix of beam shifts in X and Y from +2cm to -2cm.

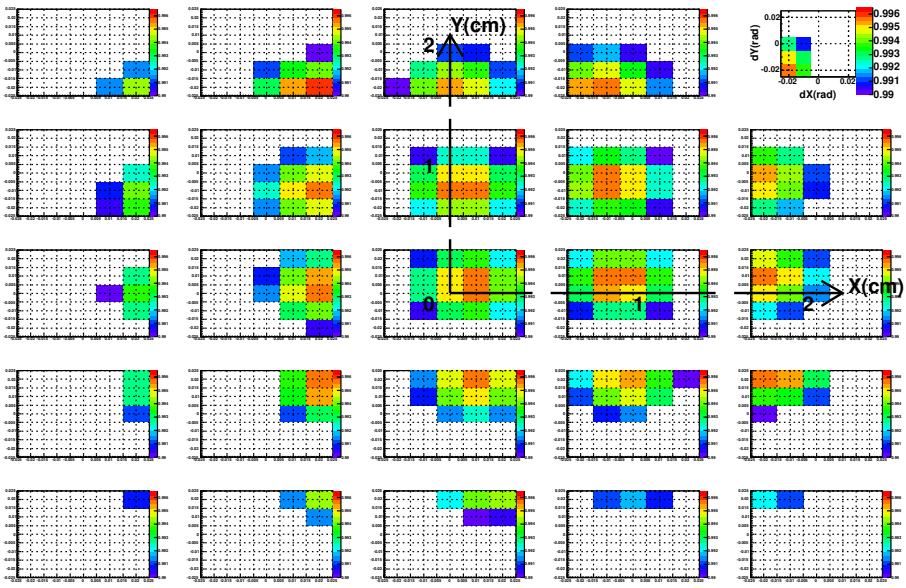

Figure 6.9: Plots showing the two dimensional quadratic fits of the polarization versus x, y, dx, and dy. The colouring and order of the plots is the same as described in Figure 6.8.

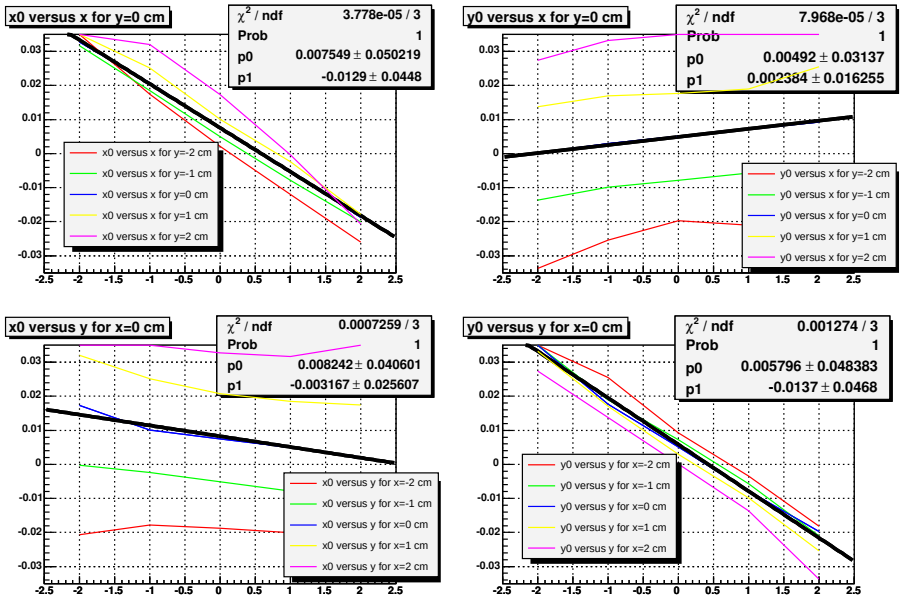

Figure 6.10: Fits of x0 versus x, x0 versus y, y0 versus x and y0 versus y used to obtain constants in the four dimensional polarization polynomial.

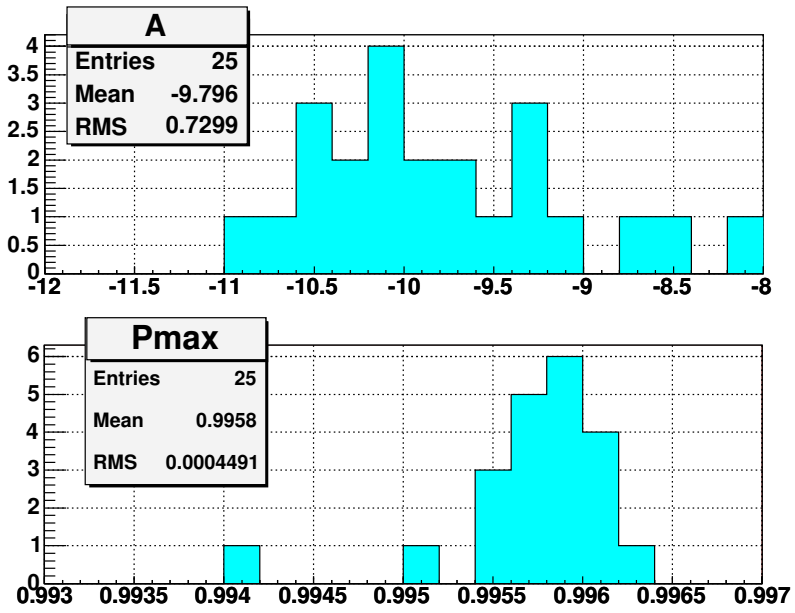

Figure 6.11: Histogram of the fit parameters A and pmax from fits to each of the 25 plots of polarization versus shift in dX and dY angle.

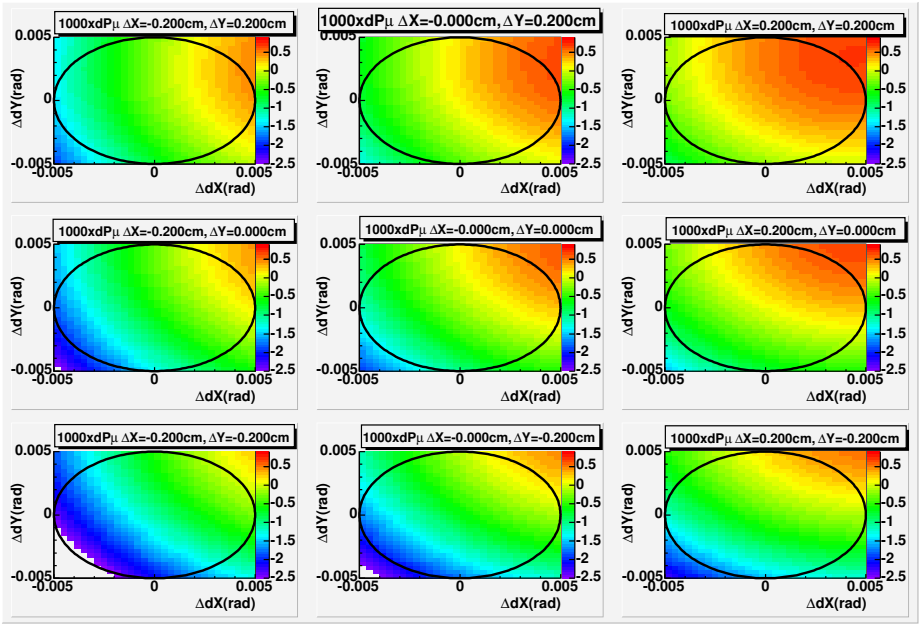

Figure 6.12: Plot used to estimate the fringe field systematic error due to uncertainty in the beam position of $\pm 2mm$, and uncertainty in the beam angle of $\pm 5mrad$.